Assessment of Tryptophan Uptake and Kinetics Using 1-(2-^{18}F-Fluoroethyl)-L-Tryptophan and α-^{11}C-Methyl-L-Tryptophan PET Imaging in Mice Implanted with Patient-Derived Brain Tumor Xenografts

Sharon K. Michelhaugh*[1], Otto Muzik*[2–4], Anthony R. Guastella*[1,5,6], Neil V. Klinger[1], Lisa A. Polin[5,6], Hancheng Cai[7], Yangchun Xin[7], Thomas J. Mangner[3,4], Shaohui Zhang[4], Csaba Juhász[2,4,6,8], and Sandeep Mittal[1,5,6]

[1]Department of Neurosurgery, Wayne State University, Detroit, Michigan; [2]Department of Pediatrics, Wayne State University, Detroit, Michigan; [3]Department of Radiology, Wayne State University, Detroit, Michigan; [4]PET Center and Translational Imaging Laboratory, Children's Hospital of Michigan, Detroit, Michigan; [5]Department of Oncology, Wayne State University, Detroit, Michigan; [6]Karmanos Cancer Institute, Detroit, Michigan; [7]Department of Radiology and Advanced Imaging Research Center, University of Texas Southwestern, Dallas, Texas; and [8]Department of Neurology, Wayne State University, Detroit, Michigan

Abnormal tryptophan metabolism via the kynurenine pathway is involved in the pathophysiology of a variety of human diseases including cancers. α-^{11}C-methyl-L-tryptophan (^{11}C-AMT) PET imaging demonstrated increased tryptophan uptake and trapping in epileptic foci and brain tumors, but the short half-life of ^{11}C limits its widespread clinical application. Recent in vitro studies suggested that the novel radiotracer 1-(2-^{18}F-fluoroethyl)-L-tryptophan (^{18}F-FETrp) may be useful to assess tryptophan metabolism via the kynurenine pathway. In this study, we tested in vivo organ and tumor uptake and kinetics of ^{18}F-FETrp in patient-derived xenograft mouse models and compared them with ^{11}C-AMT uptake. **Methods:** Xenograft mouse models of glioblastoma and metastatic brain tumors (from lung and breast cancer) were developed by subcutaneous implantation of patient tumor fragments. Dynamic PET scans with ^{18}F-FETrp and ^{11}C-AMT were obtained for mice bearing human brain tumors 1–7 d apart. The biodistribution and tumoral SUVs for both tracers were compared. **Results:** ^{18}F-FETrp showed prominent uptake in the pancreas and no bone uptake, whereas ^{11}C-AMT showed higher uptake in the kidneys. Both tracers showed uptake in the xenograft tumors, with a plateau of approximately 30 min after injection; however, ^{18}F-FETrp showed higher tumoral SUV than ^{11}C-AMT in all 3 tumor types tested. The radiation dosimetry for ^{18}F-FETrp determined from the mouse data compared favorably with the clinical ^{18}F-FDG PET tracer. **Conclusion:** ^{18}F-FETrp tumoral uptake, biodistribution, and radiation dosimetry data provide strong preclinical evidence that this new radiotracer warrants further studies that may lead to a broadly applicable molecular imaging tool to examine abnormal tryptophan metabolism in human tumors.

Key Words: glioblastoma; brain metastasis; indoleamine 2,3-dioxygenase

J Nucl Med 2017; 58:208–213
DOI: 10.2967/jnumed.116.179994

Tryptophan is an essential amino acid necessary for protein biosynthesis. Of the tryptophan not incorporated into proteins, more than 95% is metabolized via the kynurenine pathway (KP), with a smaller portion used for serotonin synthesis (Fig. 1) (*1*). The initial and rate-limiting step of the KP is the conversion of tryptophan to the central metabolite L-kynurenine and is mediated by 3 enzymes: indoleamine 2,3-dioxygenase 1 (IDO1), indoleamine 2,3-dioxygenase 2 (IDO2), and tryptophan 2,3-dioxygenase 2 (TDO2) (*2*). Kynurenine can be transformed to downstream KP metabolites including quinolinic acid, an excitotoxic glutamate receptor agonist (*2,3*). KP metabolites are implicated in the pathophysiology underlying neurodegenerative diseases such as Parkinson, Alzheimer, and Huntington disease (*3,4*). In cancer, local tryptophan depletion, kynurenine, and other KP metabolites foster an immunosuppressive tumor microenvironment (*5,6*). Recent studies have identified IDO1 in both hematologic cancers and solid tumors (e.g., breast cancer, lung cancer, glioblastoma) (*7*) with increased IDO1 expression linked to poorer outcomes (*8–10*). In addition to IDO1, TDO2 may also play a prominent role in glioma pathophysiology (*11,12*). Overall, alterations in KP enzymes and metabolites have been implicated in a wide spectrum of human diseases beyond tumors, including inflammation and psychiatric conditions (*13,14*).

To study tryptophan metabolism in vivo, the PET tracer α-^{11}C-methyl-L-tryptophan (^{11}C-AMT) can be used, because the radiolabeled methyl group prevents protein incorporation (*15*). ^{11}C-AMT PET was originally designed to estimate brain serotonin synthesis in the context of neuropsychiatric disorders (*15,16*) but also demonstrated the ability to identify epileptic foci, epileptogenic tumors, and malformations (*17,18*). ^{11}C-AMT PET studies were further extended to nonepileptogenic primary and metastatic brain tumors (*19–22*). These studies demonstrated

Received Jun. 29, 2016; revision accepted Sep. 14, 2016.
For correspondence or reprints contact: Sandeep Mittal, Department of Neurosurgery, Wayne State University, 4160 John R St., Ste. 930, Detroit, MI 48201.
E-mail: smittal@med.wayne.edu
*Contributed equally to this work.
Published online Oct. 20, 2016.

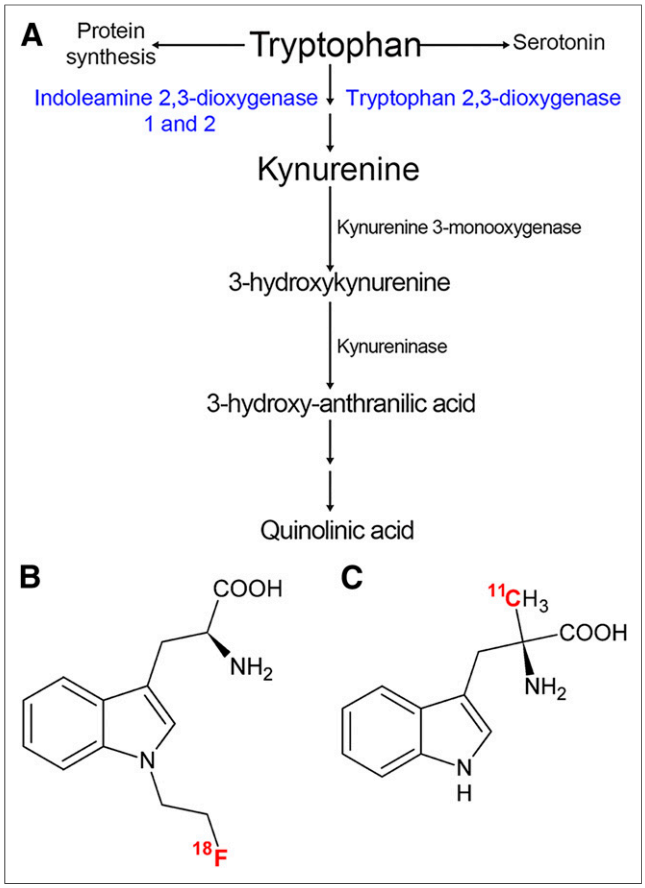

FIGURE 1. KP of tryptophan metabolism. (A) Abridged KP overview. Enzymes in blue represent rate-limiting step. (B and C) Structures of ^{18}F-FETrp and ^{11}C-AMT, respectively.

variably high ^{11}C-AMT uptake in gliomas (*18,23,24*) and meningiomas (*21*) and showed strong prognostic value for survival in patients with recurrent glioblastoma (*20*). Furthermore, ^{11}C-AMT uptake characteristics distinguished recurrent gliomas from radiation injury (*25*) and glioblastoma from metastatic brain tumors (*26*), allowing tryptophan PET imaging as a possible clinical diagnostic tool. The development of a tryptophan analog with a longer half-life isotope such as ^{18}F would permit widespread clinical application of tryptophan PET imaging.

Several novel ^{18}F-labeled tryptophan derivatives have been developed and tested as potential PET tracers for tumor imaging (*27–32*). Although most compounds showed tumor uptake, they were not designed to target IDO1, IDO12, or TDO2 activity. Most studies focused on radiosynthesis, biodistribution, or tracer transport, which could be blocked by L-type amino acid transporter 1 inhibition. Recently, 1-(2-fluoroethyl)-L-tryptophan (FETrp) was tested as a potential substrate for human IDO1 and TDO2 in in vitro enzymatic assays (*33,34*). FETrp showed variable consumption depending on the human IDO1 concentration and incubation time and appeared to be a better substrate of human IDO1 than α-D,L-methyl-tryptophan.

In this study, we tested ^{18}F-labeled FETrp (^{18}F-FETrp) as a potential PET tracer for tumor imaging by examining ^{18}F-FETrp uptake in patient-derived xenograft (PDX) mouse models of glioblastoma and brain metastases. We directly compared the tumoral uptake and tracer kinetics of ^{18}F-FETrp with those of ^{11}C-AMT using PDX models that showed ^{11}C-AMT accumulation and variable protein expression of IDO1, IDO2, and TDO2 in our recent study (*35*).

MATERIALS AND METHODS

Patient Tumor Specimens

The Wayne State University Institutional Review Board approved this study, and all subjects signed a written informed consent form. Active tumor tissue (determined by the neurosurgeon) was acquired immediately after resection and histopathologic analysis. Fragments were formalin-fixed or implanted subcutaneously into immunocompromised mice. Tumors included 2 glioblastomas, 3 breast cancer brain metastases, and 1 non–small cell lung cancer brain metastasis.

Generation of Mouse Xenograft Models

The Wayne State University Institutional Animal Care and Use Committee approved all animal experiments. Female severe combined immunodeficient BALB/c background mice (Charles River), 4- to 6-wk old, were maintained on a 12-h light–dark cycle with ad libitum food and water. Tumor fragments (~30 mg) were implanted subcutaneously, bilaterally, via trocar. Tumor growth and animal health were monitored twice weekly. Tumors were measured with Vernier calipers, and masses were estimated with the formula length × width^2/2. When the tumor burden for each mouse reached approximately 5% of its body weight, mice were euthanized and harvested tumors were serially passaged into naïve mice. Tumors

TABLE 1
Xenograft-Bearing Mouse Characteristics

Tumor ID	Tumor type	Mouse passage #	Days between scans	Right tumor (mg)*	Left tumor (mg)*	^{18}F-FETrp dose (MBq/g)	^{11}C-AMT dose (MBq/g)
14-038	Glioblastoma	7	7	344	172	0.36	1.15
14-112S	NSCLC met	5	3	351	256	0.45	1.32
15-015	Breast cancer met	5	7	320	196	0.26	1.24
15-017	Breast cancer met	8	*	300	221	0.28	†
15-037	Glioblastoma	7	1	320	221	0.40	1.19
15-070	Breast cancer met	3	4	288	304	0.38	1.30

*Tumor measurements ~2 d of ^{18}F-FETrp scans.
†^{18}F-FETrp imaging only.
NSCLC = non–small cell lung cancer; met = metastasis.

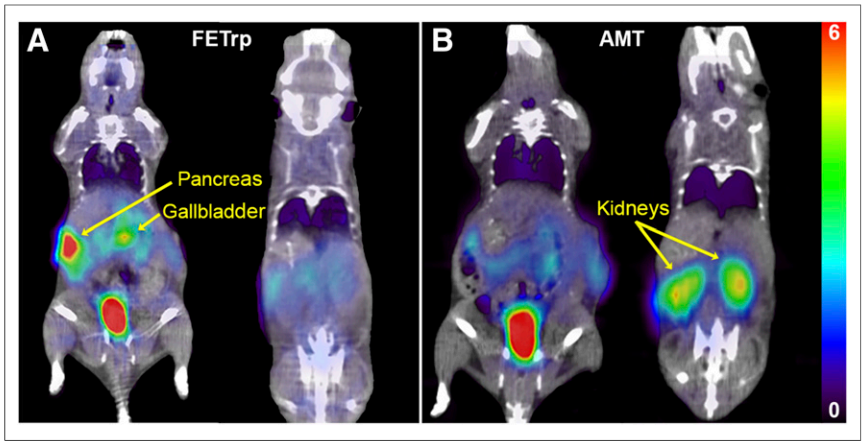

FIGURE 2. Biodistribution of ^{18}F-FETrp and ^{11}C-AMT between 30 and 60 min. Two coronal slices of 14-038 glioblastoma PDX mouse showing pancreas, gallbladder, and bladder in one plane with kidneys in other. Color scale bar represents SUV range for both tracers. (A) For ^{18}F-FETrp, high uptake is observed in both bladder and pancreas, with lesser uptake in gallbladder. Minimal uptake is seen in kidneys. (B) For ^{11}C-AMT, tracer uptake is high in bladder and kidneys, with low uptake detected in pancreas and gallbladder.

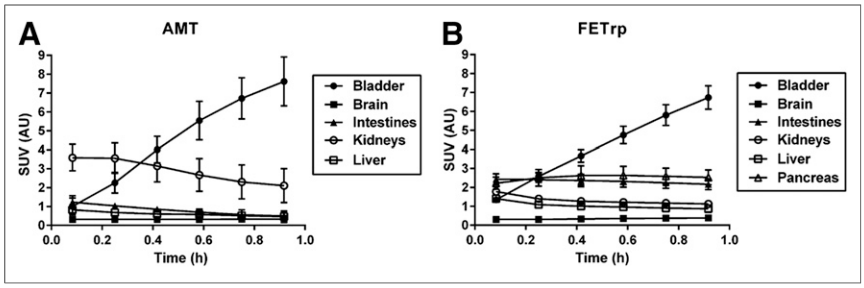

FIGURE 3. Time-dependent SUV curves characterizing ^{18}F-FETrp and ^{11}C-AMT tracers. Averaged SUVs for indicated organs (n = 5). Error bars represent SD. (A) ^{11}C-AMT tracer uptake is initially high in kidneys and undergoes washout to bladder, where activity increases with time. (B) ^{18}F-FETrp tracer shows increasing uptake in bladder, followed by relatively constant retention in pancreas and intestines. For both tracers, brain displays slow but steady accumulation.

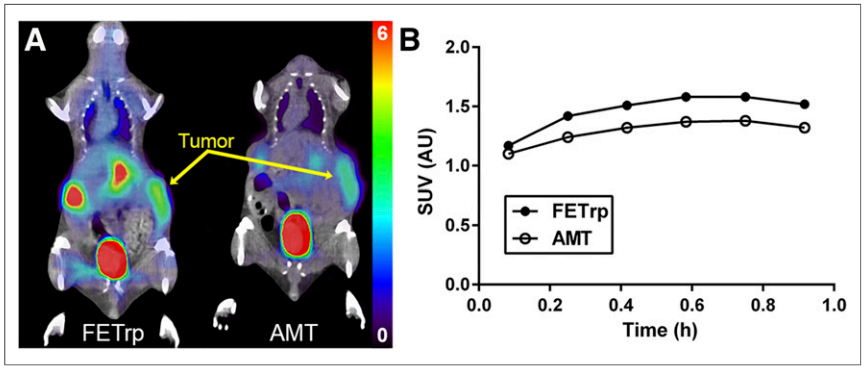

FIGURE 4. Comparison of tumoral tracer uptake between ^{18}F-FETrp and ^{11}C-AMT in the 14-038 glioblastoma PDX mouse. Mouse was injected with ^{18}F-FETrp, followed by ^{11}C-AMT 7 d later. (A) ^{18}F-FETrp tracer (left) and ^{11}C-AMT tracer (right). ^{18}F-FETrp shows increased tumoral tracer accumulation compared with ^{11}C-AMT. Color scale bar represents SUV range for both tracers. (B) Corresponding time–activity curves confirm higher tracer retention for ^{18}F-FETrp.

were passaged at least 3 times to ensure reproducible tumor growth. Harvested tumor tissues were formalin-fixed, paraffin-embedded, and sectioned at 5 μM for histology.

Radiopharmaceuticals

PET tracers were produced at the Children's Hospital of Michigan Cyclotron Facility. ^{11}C-AMT was produced as previously described (*36*). ^{18}F-FETrp was produced following published methods (*34,37*) in which ^{18}F-fluoride was produced using proton bombardment of an ^{18}O-water target. The produced ^{18}F-fluoride in ^{18}O-water was delivered and trapped on a Sep-Pak light QMA cartridge (Waters Corp.), which was eluted with a K_2CO_3/Kryptofix (Sigma Aldrich Corp.) solution (1 mg of K_2CO_3 and 6 mg of Kryptofix in 0.9 mL of acetonitrile and 0.03 mL of water). The ^{18}F solution was evaporated under a nitrogen stream at 110°C and repeated with 1.0 mL of acetonitrile. Then, a solution of ^{18}F-FETrp precursor (1.0 mg) in acetonitrile (0.25 mL) was added to the reaction vial containing dried ^{18}F ion and heated at 115°C for 5 min. After radiofluorination, hydrochloric acid (0.25 mL, 2N) was added to the vial and the mixture was heated at 115°C for 5 min. The resulting solution was diluted and passed through an alumina-N cartridge (Waters Corp.), then loaded for chiral high-performance liquid chromatography separation. The collected fraction was pH adjusted and filter sterilized. The final ^{18}F-FETrp product was a clear, colorless solution free of particulates in 5% ethanol in buffer (final pH ~5.5). Total synthesis time was approximately 50 min from the end of bombardment. The decay-corrected radiochemical yield of ^{18}F-FETrp approximated 25% at the end of synthesis. The radiochemical purity of ^{18}F-FETrp was more than 98% by the analytic chiral high-performance liquid chromatography analysis.

Small-Animal PET/CT

For each tumor model, the mouse with the greatest tumor burden from the group (n = 2–3) was imaged. Six mice were scanned with ^{18}F-FETrp. Five of these were also scanned with ^{11}C-AMT 1–7 d later (Table 1), as previously described (*35*). Mice were fasted 2–4 h before PET scanning. Scans were obtained between 11 AM and 2 PM, when tryptophan plasma levels are at the nadir in mice maintained on a 12-h light–dark cycle (*38*). Radiotracers were administered via tail vein injection. The total injected activity in mice for the ^{18}F-FETrp tracer was between 5.5 and 9.2 MBq (150–250 μCi), a dose commonly used in small-animal PET studies of mice using ^{18}F-labeled PET tracers (*39,40*). Because of the shorter half-life of the ^{11}C isotope (20 min), a higher activity was administered in the AMT study (20–22 MBq equivalent to 550–600 μCi). This dose was previously determined by our group as sufficient to obtain high-quality images in the PDX tumor models (*35*). Mice were anesthetized (1.5% isoflurane) and placed in a microPET R4 scanner (Concorde Microsystems Inc.) with an in-plane resolution of 1.76 mm in full width at

half maximum in the center of field of view and a linear resolution of less than 2.0 mm in all 3 dimensions. Approximately 5 min after tracer injection, a 60-min list-mode data acquisition in 3-dimensional mode was initiated. The list-mode data were rebinned into discrete time frames (6 × 10 min) and reconstructed using measured attenuation correction and the ordered-subsets expectation maximization iterative algorithm, yielding an isotropic resolution of approximately 2 mm in full width at half maximum. After PET scanning, a spatially corresponding CT scan was obtained using an Inveon SPECT/CT small-animal imager (Siemens Medical Solutions USA, Inc.). Food was provided to mice immediately after anesthetic recovery.

PET images were analyzed using AMIDE software (A Medical Image Data Examiner version 1.0.4) (*41*). PET and CT image volumes were coregistered by manually matching body contours in both datasets. Three-dimensional regions of interest were defined on the basis of a combination of anatomic and functional data at the tumor locations (both sides). The tracer concentration at each time point was converted to SUVs. Because time–activity curves plateaued after 30 min, data between 30 and 60 min were taken as representative of maximum tryptophan uptake for both tracers. Therefore, to characterize tumoral tryptophan accumulation, the average SUVs from 30 to 60 min were compared.

Dosimetry Calculation for ^{18}F-FETrp Radioactivity

Regions of interest for various organs were defined on serial images, and non–decay-corrected time–activity curves were obtained for the bladder, brain, gallbladder, heart, kidneys, liver, lungs, muscle, pancreas, red marrow and spleen, as identified from the CT. Time–activity curves were extended to 10 h (~5 half-lives) by extrapolating the initial dynamic scan and considering only physical decay. The residence time in each organ was calculated by integration of the area under the time–activity curve, normalized to the administered activity and multiplying the result with the organ weight. The absorbed dose to the organs was calculated assuming homogeneous distribution of radioactivity throughout the organ. The residence time of the remainder activity was accounted for by subtracting the sum of residence times determined for the organs from the inverse of the decay constant for ^{18}F (2.64 h^{-1}). Because blood is not a source organ of medical internal radionuclide dose, blood activity was assigned to the remainder of the body. Subsequently, these residence times were used together with the OLINDA software (*42*) to estimate the dose to multiple organs. The OLINDA software considers all doses from a source to a specific target organ contributed by the various decay schemes of ^{18}F (β+, electron capture) and yields the effective dose, which is representative of the overall radiation dose to a subject from PET imaging (*42,43*).

Statistical Analysis

Statistical analyses were performed with SPSS (version 22; IBM Corp.). A paired *t* test was applied to determine the significance of differences between tumor SUVs derived using both tracers. A *P* value of 0.05 or less was considered statistically significant.

RESULTS

Development and Characterization of Subcutaneous Flank Patient-Derived Xenografts

Six subcutaneous PDX models (14-038, 14-112S, 15-015, 15-017, 15-037, and 15-070) were established from patient tumor fragments (Table 1). Hematoxylin and eosin (Supplemental Fig. 1; supplemental materials are available at http://jnm.snmjournals.org) and immunohistochemical staining (Supplemental Fig. 2) were performed on all tumors, demonstrating minimal IDO1, low IDO2, moderate TDO2, and abundant L-type amino acid transporter 1 expression.

Biodistribution of Radioactivity

When at least 1 tumor on each mouse was 250 mg or more (Table 1), mice were imaged. Representative images of ^{11}C-AMT and ^{18}F-FETrp organ distribution are shown in Figure 2. For both tracers, there was prominent uptake in the bladder as they were being eliminated. ^{18}F-FETrp showed high uptake in the pancreas followed by the gallbladder, whereas ^{11}C-AMT showed prominent uptake in the kidneys. Assessment of the organ-specific time–activity curves for both tracers displayed some differences in tracer kinetics (Fig. 3). Whereas ^{11}C-AMT was rapidly extracted by the kidneys with subsequent clearance into the bladder, ^{18}F-FETrp was retained in both the pancreas and the gallbladder, and then quickly removed from the body with relatively low retention in the kidneys. Liver uptake was relatively low for both tracers, showing initially higher uptake with subsequent washout. Brain uptake was low and comparable for both tracers, showing a slow, steady increase during the scan.

Higher Tumoral ^{18}F-FETrp Tracer Uptake as Compared with ^{11}C-AMT

Both ^{11}C-AMT and ^{18}F-FETrp tracers showed PDX tumor uptake above background, with representative scans of the 14-038 glioblastoma mouse shown in Figure 4A. Corresponding SUVs demonstrated significantly higher tumor retention of ^{18}F-FETrp than ^{11}C-AMT ($P < 0.01$; Fig. 3B). Supplemental Table 1 compares SUVs obtained during the 30- to 60-min time period for ^{18}F-FETrp and ^{11}C-AMT. Overall there was higher tumoral uptake of ^{18}F-FETrp in all 3 tumor types, with the highest SUVs in glioblastomas (Fig. 5).

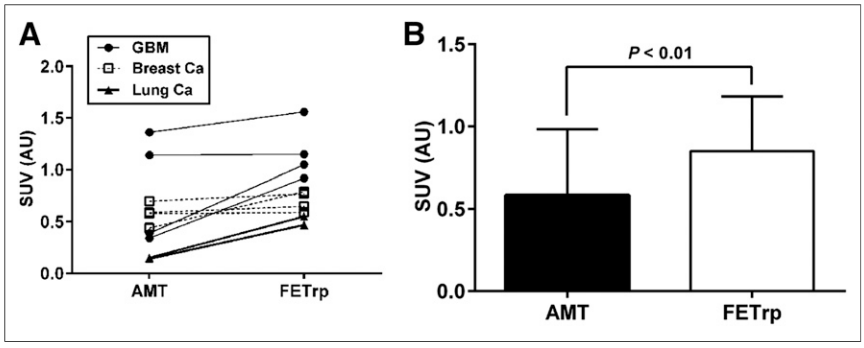

FIGURE 5. Comparison of ^{11}C-AMT and ^{18}F-FETrp PET SUVs for PDX tumors. (A) In glioblastoma, breast metastatic tumors, and non–small cell lung cancer metastatic tumors, ^{18}F-FETrp SUVs were greater than ^{11}C-AMT SUVs. (B) ^{18}F-FETrp SUVs were significantly greater than ^{11}C-AMT SUVs (paired *t* test).

Radiation Dosimetry for ^{18}F-FETrp

The residence times were calculated from kinetic ^{18}F-FETrp PET data (Supplemental Table 2), and organ-absorbed radiation dose estimates in humans were calculated (Supplemental Table 3). The results indicate that the critical organ is the pancreas (~160 μSv/MBq), followed by the bladder (~150 μSv/MBq). Finally, we determined that administration of 5 MBq/kg (0.14 mCi/kg) of ^{18}F-FETrp for PET studies would result in a total PET dose of approximately 8 mSv in human subjects (Table 2).

TABLE 2
Radiation Absorbed Dose from ^{18}F-FETrp PET Studies in Adult Control Subjects

Subject	Effective dose (μSv/MBq [rem/mCi])	Critical organ, pancreas (μSv/MBq [rad/mCi])	Effective PET dose (mSv [rem])
Control male (70 kg)	20.9 (0.077)	151 (0.557)	7.3 (0.756)
Control female (57 kg)	23.2 (0.086)	168 (0.621)	8.1 (0.843)

For injected activity of 5 MBq/kg (0.14 mCi/kg).

DISCUSSION

This study had 3 major findings. First, we demonstrated the biodistribution of ^{18}F-FETrp in a mouse model, which was somewhat different from what is typically seen on ^{11}C-AMT PET; second, we showed accumulation of ^{18}F-FETrp in PDXs of different human tumors, with mean ^{18}F-FETrp SUVs exceeding ^{11}C-AMT uptake by 30% or more in the same tumors, depending on the tumor type. Finally, our radiation dosimetry data indicate pancreas and bladder to be the critical organs for ^{18}F-FETrp, with the estimated total PET dose of 8 mSv in humans.

The most apparent differences in organ distribution between the 2 tracers include the higher pancreas and lower kidney uptake of ^{18}F-FETrp than ^{11}C-AMT. The reason for these differences is currently unclear and will require further studies. ^{18}F-FETrp shows no appreciable bone accumulation, suggesting negligible defluorination (*44*). The observed organ radioactivities may arise mostly from unmetabolized radiotracers, although this will require further studies. Nevertheless, the high ^{18}F-FETrp uptake in the bladder and pancreas suggests that this tracer would not allow visualization of tumors in these organs because of high background activity. Despite the differences in distribution, both tracers demonstrated similarly low and continuous brain accumulation, suggesting that ^{18}F-FETrp will be suitable for the imaging of intracranial brain tumors as previously established with ^{11}C-AMT (*18–26*).

The substantially higher uptake of ^{18}F-FETrp than ^{11}C-AMT in all 3 tumor types is promising, suggesting that ^{18}F-FETrp could be useful for imaging tryptophan uptake and kinetics in these human tumors. Our previous PET studies demonstrated differential ^{11}C-AMT transport and trapping in human gliomas, lung cancer, and breast cancer, tumors that expressed both the L-type amino acid transporter 1 and IDO1 (*23,26,45–47*). However, the widespread use of ^{11}C-AMT for cancer imaging is not feasible because of its short half-life and tedious radiosynthesis. The current findings suggest that ^{18}F-FETrp may not only overcome these limitations but also provide a better tumor-to-background ratio. Importantly, ^{18}F-FETrp could also be useful to estimate tryptophan metabolism via IDO1, IDO2, or TDO2. This is supported by in vitro data demonstrating markedly higher ^{18}F-FETrp accumulation in IDO1-expressing P815B-mIDO1 cl6 cells than in P815B-IDO1–negative cl1 cells (*33,34*). Notably, high ^{18}F-FETrp accumulation in P815B-mIDO1 cl6 cells was blocked by 1-methyl-L-tryptophan, an IDO1 inhibitor, suggesting this radiotracer is a promising candidate for imaging in vivo IDO1 enzyme activity. Noninvasive estimation of tumoral IDO1 activity would be critical for patient stratification and treatment monitoring in clinical trials using IDO1 inhibitors developed to overcome tumoral immune resistance via the upregulated KP (*48,49*). A clinicaltrials.gov search (search terms IDO, cancer; May 11, 2016) yielded more than 20 open, active, or completed studies using IDO1-targeted drugs in cancer. Most of these included epacodostat or indoximod in conjunction with standard chemotherapies for the treatment of solid tumors such as glioblastoma, non–small cell lung cancer, and breast cancer, further underscoring the potential clinical utility of ^{18}F-FETrp PET imaging. The tumor models in the present study showed stronger expression of IDO2 and TDO2 than IDO1, suggesting that ^{18}F-FETrp PET may be useful to monitor activity of these enzymes. Whether or not in vivo uptake values can estimate KP enzyme activity will need to be determined.

Finally, the effective dose of the ^{18}F-FETrp tracer was found to be approximately 20% lower than the effective dose of ^{18}F-FDG PET tracer (8 vs. 10 mSv, respectively) (*50*), which is the standard clinical tracer for cancer PET imaging. The average ^{18}F-FETrp dose to the critical organ, the pancreas, is only about 75% of ^{18}F-FDG to its critical organ, the urinary bladder (160 μSv/MBq vs. 220 μSv/MBq, respectively). Collectively, our data indicate that the overall radiation dose for a PET study using ^{18}F-FETrp compares favorably with the clinical ^{18}F-FDG tracer. Importantly, a recent study reported a simplified, fully automated synthesis of ^{18}F-FETrp (*34*), making this a potentially attractive radiotracer for widespread clinical use.

CONCLUSION

Although limited to PDX mouse models, our study provides strong preliminary evidence for the potential clinical value of ^{18}F-FETrp PET. Future studies should evaluate this radiotracer for imaging in vivo tumoral IDO1 activity. Studies using ^{18}F-FETrp PET in patients to image both brain and extracranial tumors are clearly warranted and may lead to a new, broadly available noninvasive diagnostic and prognostic clinical tool.

DISCLOSURE

The study was supported by grant R01CA123451 (Csaba Juhász and Sandeep Mittal) from the National Cancer Institute; by the Fund for Medical Research and Education, Wayne State University School of Medicine (Sandeep Mittal); and a Strategic Research Initiative Grant from Karmanos Cancer Institute (Sandeep Mittal and Csaba Juhász). Anthony R. Guastella is supported by the Initiative to Maximize Student Development Fellowship (Wayne State University). The Animal Model and Therapeutics Evaluation Core; the Microscopy, Imaging and Cytometry Resources Core; and Biobanking and Correlative Sciences Core are supported, in part, by NIH Center grant P30CA022453 to the Karmanos Cancer Institute at Wayne State University. No other potential conflict of interest relevant to this article was reported.

ACKNOWLEDGMENTS

We thank Xin Lu, MS, and Kirk Douglas, BS, for performing the small-animal PET/CT studies.

REFERENCES

1. Peters JC. Tryptophan nutrition and metabolism: an overview. *Adv Exp Med Biol.* 1991;294:345–358.
2. Badawy AA. Tryptophan availability for kynurenine pathway metabolism across the life span: control mechanisms and focus on aging, exercise, diet and nutritional supplements. *Neuropharmacology.* November 23, 2015 [Epub ahead of print].
3. Majewski M, Kozlowska A, Thoene M, Lepiarczyk E, Grzegorzewski WJ. Overview of the role of vitamins and minerals on the kynurenine pathway in health and disease. *J Physiol Pharmacol.* 2016;67:3–19.
4. Lovelace MD, Varney B, Sundaram G, et al. Recent evidence for an expanded role of the kynurenine pathway of tryptophan metabolism in neurological diseases. *Neuropharmacology.* March 16, 2016 [Epub ahead of print].
5. Frumento G, Rotondo R, Tonetti M, Damonte G, Benatti U, Ferrara GB. Tryptophan-derived catabolites are responsible for inhibition of T and natural killer cell proliferation induced by indoleamine 2,3-dioxygenase. *J Exp Med.* 2002;196: 459–468.
6. Fallarino F, Grohmann U, You S, et al. The combined effects of tryptophan starvation and tryptophan catabolites down-regulate T cell receptor zeta-chain and induce a regulatory phenotype in naive T cells. *J Immunol.* 2006;176:6752–6761.
7. Moon YW, Hajjar J, Hwu P, Naing A. Targeting the indoleamine 2,3-dioxygenase pathway in cancer. *J Immunother Cancer.* 2015;3:51.
8. Brandacher G, Perathoner A, Ladurner R, et al. Prognostic value of indoleamine 2,3-dioxygenase expression in colorectal cancer: effect on tumor-infiltrating T cells. *Clin Cancer Res.* 2006;12:1144–1151.
9. Astigiano S, Morandi B, Costa R, et al. Eosinophil granulocytes account for indoleamine 2,3-dioxygenase-mediated immune escape in human non-small cell lung cancer. *Neoplasia.* 2005;7:390–396.
10. Takao M, Okamoto A, Nikaido T, et al. Increased synthesis of indoleamine-2,3-dioxygenase protein is positively associated with impaired survival in patients with serous-type, but not with other types of, ovarian cancer. *Oncol Rep.* 2007; 17:1333–1339.
11. Adams S, Teo C, McDonald KL, et al. Involvement of the kynurenine pathway in human glioma pathophysiology. *PLoS One.* 2014;9:e112945.
12. Opitz CA, Litzenburger UM, Sahm F, et al. An endogenous tumour-promoting ligand of the human aryl hydrocarbon receptor. *Nature.* 2011;478:197–203.
13. Vécsei L, Szalardy L, Fulop F, Toldi J. Kynurenines in the CNS: recent advances and new questions. *Nat Rev Drug Discov.* 2013;12:64–82.
14. Mittal S, ed. *Targeting the Broadly Pathogenic Kynurenine Pathway.* 1st ed. New York, New York: Springer International Publishing Switzerland; 2015.
15. Diksic M, Tohyama Y, Takada A. Brain net unidirectional uptake of alpha-[^{14}C] methyl-L-tryptophan (alpha-MTrp) and its correlation with regional serotonin synthesis, tryptophan incorporation into proteins, and permeability surface area products of tryptophan and alpha-MTrp. *Neurochem Res.* 2000;25:1537–1546.
16. Diksic M, Young SN. Study of the brain serotonergic system with labeled alpha-methyl-L-tryptophan. *J Neurochem.* 2001;78:1185–1200.
17. Juhász C, Chugani DC, Muzik O, et al. Alpha-methyl-L-tryptophan PET detects epileptogenic cortex in children with intractable epilepsy. *Neurology.* 2003;60:960–968.
18. Alkonyi B, Mittal S, Zitron I, et al. Increased tryptophan transport in epileptogenic dysembryoplastic neuroepithelial tumors. *J Neurooncol.* 2012;107:365–372.
19. Juhász C, Dwivedi S, Kamson DO, Michelhaugh SK, Mittal S. Comparison of amino acid positron emission tomographic radiotracers for molecular imaging of primary and metastatic brain tumors. *Mol Imaging.* 2014;13:1–16.
20. Kamson DO, Mittal S, Robinette NL, et al. Increased tryptophan uptake on PET has strong independent prognostic value in patients with a previously treated high-grade glioma. *Neuro-oncol.* 2014;16:1373–1383.
21. Bosnyák E, Kamson DO, Guastella AR, et al. Molecular imaging correlates of tryptophan metabolism via the kynurenine pathway in human meningiomas. *Neuro-oncol.* 2015;17:1284–1292.
22. Bosnyák E, Kamson DO, Robinette NL, Barger GR, Mittal S, Juhasz C. Tryptophan PET predicts spatial and temporal patterns of post-treatment glioblastoma progression detected by contrast-enhanced MRI. *J Neurooncol.* 2016;126:317–325.
23. Juhász C, Chugani DC, Muzik O, et al. In vivo uptake and metabolism of alpha-[^{11}C]methyl-L-tryptophan in human brain tumors. *J Cereb Blood Flow Metab.* 2006;26:345–357.
24. Juhász C, Muzik O, Chugani DC, et al. Differential kinetics of alpha-[^{11}C] methyl-L-tryptophan on PET in low-grade brain tumors. *J Neurooncol.* 2011;102:409–415.
25. Alkonyi B, Barger GR, Mittal S, et al. Accurate differentiation of recurrent gliomas from radiation injury by kinetic analysis of alpha-^{11}C-methyl-L-tryptophan PET. *J Nucl Med.* 2012;53:1058–1064.
26. Kamson DO, Mittal S, Buth A, et al. Differentiation of glioblastomas from metastatic brain tumors by tryptophan uptake and kinetic analysis: a positron emission tomographic study with magnetic resonance imaging comparison. *Mol Imaging.* 2013;12:327–337.
27. Chiotellis A, Muller A, Mu L, et al. Synthesis and biological evaluation of ^{18}F-labeled fluoroethoxy tryptophan analogues as potential PET tumor imaging agents. *Mol Pharm.* 2014;11:3839–3851.
28. He S, Tang G, Hu K, et al. Radiosynthesis and biological evaluation of 5-(3-[^{18}F] fluoropropyloxy)-L-tryptophan for tumor PET imaging. *Nucl Med Biol.* 2013;40: 801–807.
29. Krämer SD, Mu L, Muller A, et al. 5-(2-^{18}F-fluoroethoxy)-L-tryptophan as a substrate of system L transport for tumor imaging by PET. *J Nucl Med.* 2012;53:434–442.
30. Li R, Wu SC, Wang SC, Fu Z, Dang Y, Huo L. Synthesis and evaluation of l-5-(2-[^{18}F]fluoroethoxy)tryptophan as a new PET tracer. *Appl Radiat Isot.* 2010; 68:303–308.
31. Shih IH, Duan XD, Kong FL, et al. Automated synthesis of ^{18}F-fluoropropoxytryptophan for amino acid transporter system imaging. *Biomed Res Int.* 2014;2014:492545.
32. Weiss PS, Ermert J, Castillo Melean J, Schafer D, Coenen HH. Radiosynthesis of 4-[^{18}F]fluoro-L-tryptophan by isotopic exchange on carbonyl-activated precursors. *Bioorg Med Chem.* 2015;23:5856–5869.
33. Henrottin J, Zervosen A, Lemaire C, et al. N (1)-fluoroalkyltryptophan analogues: synthesis and in vitro study as potential substrates for indoleamine 2,3-dioxygenase. *ACS Med Chem Lett.* 2015;6:260–265.
34. Henrottin J, Lemaire C, Egrise D, et al. Fully automated radiosynthesis of N1-[^{18}F]fluoroethyl-tryptophan and study of its biological activity as a new potential substrate for indoleamine 2,3-dioxygenase PET imaging. *Nucl Med Biol.* 2016;43: 379–389.
35. Guastella AR, Michelhaugh SK, Klinger NV, et al. Tryptophan PET imaging of the kynurenine pathway in patient-derived xenograft models of glioblastoma. *Mol Imaging.* 2016;15:1–11.
36. Chakraborty PK, Mangner TJ, Chugani DC, Muzik O, Chugani HT. A high-yield and simplified procedure for the synthesis of alpha-[^{11}C]methyl-L-tryptophan. *Nucl Med Biol.* 1996;23:1005–1008.
37. Sun T, Tang G, Tian H, et al. Radiosynthesis of 1-[^{18}F]fluoroethyl-L-tryptophan as a novel potential amino acid PET tracer. *Appl Radiat Isot.* 2012;70:676–680.
38. Feigin RD, Dangerfield HG, Beisel WR. Circadian periodicity of blood amino acids in normal and adrenalectomized mice. *Nature.* 1969;221:94–95.
39. Chang CH, Jan ML, Fan KH, et al. Longitudinal evaluation of tumor metastasis by an FDG-microPet/microCT dual-imaging modality in a lung carcinoma-bearing mouse model. *Anticancer Res.* 2006;26:159–166.
40. Dandekar M, Tseng JR, Gambhir SS. Reproducibility of ^{18}F-FDG microPET studies in mouse tumor xenografts. *J Nucl Med.* 2007;48:602–607.
41. Loening AM, Gambhir SS. AMIDE: a free software tool for multimodality medical image analysis. *Mol Imaging.* 2003;2:131–137.
42. Stabin MG, Sparks RB, Crowe E. OLINDA/EXM: the second-generation personal computer software for internal dose assessment in nuclear medicine. *J Nucl Med.* 2005;46:1023–1027.
43. Stabin MG. MIRDOSE: personal computer software for internal dose assessment in nuclear medicine. *J Nucl Med.* 1996;37:538–546.
44. Fiserova-Bergerova V. Changes of fluoride content in bone: an index of drug defluorination in vivo. *Anesthesiology.* 1973;38:345–351.
45. Batista CE, Juhasz C, Muzik O, et al. Imaging correlates of differential expression of indoleamine 2,3-dioxygenase in human brain tumors. *Mol Imaging Biol.* 2009;11:460–466.
46. Juhász C, Nahleh Z, Zitron I, et al. Tryptophan metabolism in breast cancers: molecular imaging and immunohistochemistry studies. *Nucl Med Biol.* 2012;39: 926–932.
47. Juhász C, Muzik O, Lu X, et al. Quantification of tryptophan transport and metabolism in lung tumors using PET. *J Nucl Med.* 2009;50:356–363.
48. Vacchelli E, Aranda F, Eggermont A, et al. Trial watch: IDO inhibitors in cancer therapy. *OncoImmunology.* 2014;3:e957994.
49. Collin M. Immune checkpoint inhibitors: a patent review (2010-2015). *Expert Opin Ther Pat.* 2016;26:555–564.
50. Hays MT, Watson EE, Thomas SR, Stabin M. MIRD dose estimate report no. 19: radiation absorbed dose estimates from ^{18}F-FDG. *J Nucl Med.* 2002;43:210–214.